Applied Catalysis B: Environmental 162 (2015) 57–65

Contents lists available at ScienceDirect

Applied Catalysis B: Environmental

journal homepage: www.elsevier.com/locate/apcatb

Multifunctionality of Cu–ZnO–ZrO_2/H-ZSM5 catalysts for the one-step CO_2-to-DME hydrogenation reaction

F. Frusteri, M. Cordaro, C. Cannilla, G. Bonura*

CNR-ITAE, Institute for Advanced Energy Technologies "Nicola Giordano", Via S. Lucia sopra Contesse, 5, 98126 Messina, Italy

ARTICLE INFO

Article history:
Received 28 April 2014
Received in revised form 16 June 2014
Accepted 19 June 2014
Available online 26 June 2014

Keywords:
CO_2 hydrogenation
Dimethyl ether
Cu–ZnO–ZrO_2 catalysts
Zeolites

ABSTRACT

A series of Cu–ZnO–ZrO_2/H-ZSM5 multifunctional catalysts for the one-step CO_2-to-DME hydrogenation reaction was prepared *via* coprecipitation of methanol catalyst precursors by means of different precipitating agents (*i.e.*, sodium bicarbonate, ammonium carbonate, oxalic acid and urea) in a slurry containing dispersed zeolite particles. The samples were characterized by XRF, XRD, N_2 adsorption/desorption isotherms, SEM, N_2O-titration, TPR and NH_3/CO_2 TPD techniques, while the catalytic testing was carried out in a fixed-bed reactor operating at 3.0 MPa, in the T_R range 473–513 K and space velocity of 10,000 h^{-1} ($CO_2/H_2/N_2$, 3/9/1). The experiments revealed that the preparation methodology significantly affects catalyst properties and hence catalyst activity. The multifunctional catalyst prepared *via* ammonium carbonate precipitation resulted to be the most active in CO_2 conversion, also accomplishing high DME selectivity, with a maximum space-time yield of 0.225 $kg_{DME}/kg_{cat}/h$. Catalyst characterization disclosed that the strength of basic sites, the ratio between acid and basic sites along with the Cu particle sizes are crucial to achieve maximum catalytic performance, keeping CO selectivity to a minimum value.

1. Introduction

The chemical transformation of CO_2 into useful products and fuels, *e.g.*, methanol (MeOH), dimethyl ether (DME), urea, hydrocarbons, etc., is an attractive way of recycling CO_2 and thereby controlling its emission into the atmosphere [1–4]. In particular, DME is considered a prospective "future fuel", usable either as a starting material for the production of a range of chemicals, such as oxygenates, olefins and hydrocarbon fuels (gasoline, jet fuel), or as an efficient H_2 carrier for fuel cells and other applications [4–7].

Conventionally, DME is produced through a two-step process, according to which methanol is first synthesized from syngas (*i.e.*, $CO + H_2$); then, DME is produced from the dehydration of methanol [8–10]. As an alternative, the one-step process integrates the synthesis of methanol and its dehydration to DME into a single step, so increasing the driving force for CO_2 conversion and taking economically advantage from the need of only one reactor rather than two [11,12]. So, catalysts for the direct CO_2-to-DME process should be able to efficiently catalyze both methanol synthesis (MS) and methanol dehydration (MD) reactions, while the yield of CO, formed *via* the RWGS side reaction [13,14], should be kept to a minimum. Typically, MS reaction is carried out on Cu–ZnO–Al_2O_3 catalysts, although Cu–ZnO–ZrO_2 catalysts are recently claimed as more active catalytic systems due to a better water tolerance of zirconia with respect to alumina [15–19], whereas MD reaction takes place fast over a solid acid component.

Although some recent paper documents that a relatively high productivity could be achieved upon physical or mechanical mixing between the methanol catalyst and the acid catalyst [20,21], the need for a relatively higher degree of inter-dispersion among the components pushes the scientific interest toward the integration of a multi-functionality necessary for reaction over a single catalyst, so to realize a more efficient mass transfer rate from the metal–oxide sites of methanol production to the acid sites of methanol dehydration [22].

In this work, "multifunctional catalyst" refers to a system where the catalytic functionalities necessary for the direct CO_2-to-DME hydrogenation reaction are chemically combined during the preparation step, so giving a "homogeneous" novel system in which the two parent catalysts are not distinguishable anymore. The influence of different preparation procedures is assessed, in order to optimize the system in terms of physico-chemical properties and catalytic activity in the direct DME synthesis from CO_2/H_2 mixtures.

* Corresponding author. Tel.: +39 090 624 205; fax: +39 090 624 247.
E-mail address: giuseppe.bonura@itae.cnr.it (G. Bonura).

http://dx.doi.org/10.1016/j.apcatb.2014.06.035
0926-3373/

2. Experimental

2.1. Catalyst preparation

The preparation procedure of all multifunctional systems consists in the generation of the methanol catalyst directly in a solution containing a zeolite (*CBV3024E*, Zeolyst Int., SiO_2/Al_2O_3 = 30 mol/mol) finely dispersed (particle size <100 μm). So, during precipitation of the metal precursors, the zeolite will result "englobed", so generating a system containing both metal–oxide sites (characteristic of methanol catalyst) and acid sites (typical of H-zeolite). In such systems, the methanol precursors are present with a $CuO/ZnO/ZrO_2$ weight ratio of ca. 3/1/3, whereas the zeolite weight was calculated considering a 1:1 ratio with respect to the methanol catalyst functionality.

Four different procedures were developed, as described in the following:

(1) *Coprecipitation of the methanol catalyst precursors by $NaHCO_3$ and deposition on the zeolite particles in aqueous medium (ZZ-CC).* An appropriate amount of copper, zinc and zirconium nitrate precursors, by Sigma Aldrich, was solubilized in 50 mL of water. The H-ZSM5 zeolite was finely dispersed in 500 mL of a 0.2 M $NaHCO_3$ solution. Then, the solution containing the precursors was added, in a slow and constant mode, to the $NaHCO_3$ solution containing the zeolite at 353 K, under vigorous stirring and ultrasonic irradiation, so to enhance the textural properties of the catalyst, especially in terms of surface area and porosity [19,23]. The pH of the solution was kept in the range of 7.0–7.5 with continuous addition of $NaHCO_3$ (1.0 M) to ensure the formation of carbonates. After the precipitation, the green solid was left at 353 K, under stirring and ultrasound irradiation for 2 h. The precipitate was repeatedly washed with hot distilled water to remove Na^+ ions, dried at 383 K for 16 h and then calcined at 623 K for 4 h, according to the stepwise procedure elsewhere reported [24].

(2) *Coprecipitation of the methanol catalyst precursors by $(NH_4)_2CO_3$ and deposition on the zeolite particles in aqueous medium (ZZ-NC).* An aqueous solution (50 mL) of copper, zinc and zirconium nitrate precursors, by Sigma Aldrich, were added, in a slow and constant mode, to a $(NH_4)_2CO_3$ solution (500 mL, 0.2 M) containing the zeolite finely dispersed, at 353 K, under vigorous stirring and ultrasonic irradiation. The pH of the solution was kept in the range of 7.0–7.5 with continuous additions of $(NH_4)_2CO_3$ (1.0 M) to ensure the formation of carbonates. During the precipitation step, the solution got an intense blue color. After the precipitation, the sky–blue solid was left at 353 K, under stirring and ultrasound irradiation for 2 h, washed with hot distilled water and dried at 383 K for 16 h and then calcined at 623 K for 4 h, according to the stepwise procedure elsewhere reported [24].

(3) *Coprecipitation of the methanol catalyst precursors by oxalic acid and deposition on the zeolite particles in ethanolic medium (ZZ-OC).* $Cu(NO_3)_2{\cdot}2{,}5H_2O$ (3.2 g), $Zn(NO_3)_2{\cdot}6H_2O$ (1.4 g) and $ZrO(NO_3)_2{\cdot}nH_2O$ (6.0 g), by Sigma Aldrich, were solubilized in 50 ml of ethanol. Then, the solution of precursors was added, at room temperature and in a slow and constant mode, to a vigorously stirred ethanolic solution containing ca. 4.0 g of oxalic acid (20 wt.% in excess with respect to the stoichiometric amount necessary to precipitate the metal precursors) and the powdered zeolite in a 1:1 weight ratio with respect to the final oxide composition of the methanol catalyst. The precipitate was mixed for 3 h, then aged overnight. The catalyst was filtered, dried at 383 K for 16 h and then calcined at 623 K for 4 h, according to the stepwise procedure elsewhere reported [24].

(4) *Urea hydrolysis of the methanol catalyst precursors and deposition on the zeolite particles in aqueous medium (ZZ-UH).* The copper, zinc and zirconium nitrate precursors, by Sigma Aldrich, were solubilized in 600 mL of water. Urea, in a fivefold molar concentration with respect to the precursors, was added at the aqueous solution, until complete solubilization. Then, the zeolite was finely dispersed. The obtained suspension was stirred for 30 min at room temperature. The initial pH was 4.84. Then, the solution was heated at 373 K, so reaching a minimum pH of 2.49. After 3 h, the pH reached neutral value and solution assumed an intense blue color. The reaction was stopped and the precipitate was filtered, washed and then dried at 383 K for 16 h. Finally, it was calcined at 623 K for 4 h, according to the stepwise procedure elsewhere reported [24].

2.2. Catalysts characterization

2.2.1. X-rays fluorescence (XRF) measurements

The analytical composition of Cu based catalysts were determined by XRF measurements, using a Bruker AXS—S4 Explorer spectrometer, equipped with a Rhodium X-ray source (Rh anode and 75 μm Be-window), a LiF 220 crystal analyzer and a 0.12° divergence collimator. The analytical composition of the catalysts was expressed in percentage by weight of oxides.

2.2.2. Total surface area (SA_{BET}) measurements

The textural properties of catalysts were determined by physical adsorption measurements of nitrogen to its boiling point (77 K), using a Micromeritics ASAP 2020 gas adsorption device. The isotherms were elaborated for assessment of surface area (*SA*) and porosity (*PV*), with the micropore volume (V_{micro}) determined by the *t*-plot approach.

2.2.3. X-rays diffraction (XRD) measurements

XRD patterns of catalysts were obtained by a Philips X-Pert diffractometer operating at 40 kV and 30 mA, employing the Ni β-filtered Cu *K*α radiation (λ = 1.5406 Å) in the 2θ range 10–80°. Identification of XRD patterns was made on the basis of the JCPDS database, while the metal particle size was determined by Scherrer equation assuming a Gaussian shape of the peaks.

2.2.4. Temperature Programmed Reduction (TPR) measurements

The measurements of reducibility were performed in hydrogen atmosphere using a linear quartz micro-reactor (*i.d.*, 4 mm) fed with a 5 vol.% H_2/Ar at the flow rate of 30 *STP* mL/min. The experiments were carried out in the range 273–1173 K with a heating rate of 20 K/min. The hydrogen consumption was monitored by a thermal conductivity detector (TCD), previously calibrated with a known amount of a commercial CuO standard. TPR data resulted very reproducible both in the maximum position (±3 K) and extent of H_2 consumption (±3%).

2.2.5. N_2O titration measurements

Copper surface area (S_{Cu}) and dispersion (D_{Cu}) values were obtained by "single-pulse" N_2O-titration measurements at 363 K [25]. Before measurements the samples were reduced *in situ* at 573 K in flowing H_2 (100 *STP* mL/min) for 1 h, then "flushed" at 583 K in nitrogen carrier flow (15 min) and further cooled down at 363 K. S_{Cu} and D_{Cu} values were calculated assuming a $Cu{:}N_2O$ = 2:1 titration stoichiometry and a surface atomic density of 1.46×10^{19} Cu_{at}/m^2, while, assuming a spherical shape, the Cu average particle size (d_{Cu}) was obtained from the conventional formula [25]: d_{Cu} (nm) = $104/D_{Cu}$ (%).

2.2.6. Temperature programmed desorption of NH_3 (NH_3-TPD)

NH_3-TPD measurements for the surface acidity determination were performed by using 100 mg of sample in a linear quartz micro-reactor (*i.d.*, 4 mm; *l.*, 200 mm), with a helium carrier flow of 25 *STP* mL/min. The experiments were carried out in the range 373–973 K with a heating rate of 10 K/min. The ammonia desorption was monitored by TCD, calibrated by the peak area of known pulses of NH_3. Prior of each measurements, the sample was pretreated at 573 K with hydrogen flowing at 100 mL/min for 1 h and then cooled down to 423 K and saturated at a flow rate of 25 mL/min for 1.5 h with a 5 vol.% NH_3/He stream. Then, the samples were purged in He atmosphere for ca. 1 h until a constant TCD level was obtained.

2.2.7. Temperature programmed desorption of CO_2 (CO_2-TPD)

CO_2-TPD were carried out in the range 373–1073 K with a heating rate of 10 K/min, using He as carrier gas (25 mL/min). Pre-reduced catalysts were cooled to room temperature and further saturated in CO_2 flow (25 mL/min) for 60 min at 473 K. CO_2 (*m*/*z*, 44) desorption process was monitored by a ThermoLab Quadrupole Mass Spectrometer. CO_2 peak area was quantitatively calibrated by injecting CO_2 calibrating pulses.

2.2.8. Scanning electron microscopy (SEM) assisted with energy dispersive X-ray analysis (EDAX)

SEM-EDAX analysis was carried out to study the morphology of the catalyst surface and also to analyze the atomic composition on the examined surface. SEM analysis was made by using a Philips XL-30-FEG microscope with an accelerating voltage of 5 kV, fitted with an EDAX analyzer (Oxford, model 6587). Specimens were prepared by gold sputtering of catalyst samples deposited as powders on aluminum pin flat stubs.

2.3. Catalyst testing

The catalytic activity was investigated in a fixed-bed stainless steel reactor (*i.d.*, 4 mm; *l.*, 200 mm) at temperature ranging from 453 to 513 K and a total pressure of 3.0 MPa (F = 2.4 *STP* L/h; $CO_2/H_2/N_2$ = 3/9/1), using 0.25 g of multifunctional catalyst (40–70 mesh), diluted with granular SiC (0.25 g). Prior to each test, the catalyst was reduced *in situ* at 573 K for 1 h in pure hydrogen flow at atmospheric pressure. The reaction stream was analyzed by a GC equipped with a two-column separation system connected to a *flame ionized detector* (FID) and *thermal conductivity detector* (TCD), respectively. Conversion-selectivity data were calculated by both internal standard and mass-balance methods [14], each data set being obtained, with an accuracy of ±3%, from an average of three independent measurements.

3. Results and discussion

3.1. Textural properties

The analytic compositions of each catalyst along with surface area and pore volume are reported in Table 1. As the ratio between copper, zinc, zirconium precursors and H-ZSM5 zeolite was maintained constant for each system, the weight composition only slightly differs among them: in general, the metal–oxide/zeolite ratio is roughly 50.5/49.5 wt.%.

Notwithstanding the accurate washing procedure employed, the ZZ-CC sample contains 1.6 wt.% of residual Na, as the result of the ionic exchange of H-atoms of zeolite with sodium occurring during preparation step.

Also the textural properties of the catalysts differ from each other. In fact, while the ZZ-OC system prepared by gel-oxalate coprecipitation exhibits a surface area of 248 m^2/g and a cumulative pore volume of 0.261 cm^3/g, the ZZ-UH sample, prepared by urea hydrolysis, shows higher area exposure (*SA*, 372 m^2/g) and pore volume (*PV*, 0.286 cm^3/g). The textural properties of ZZ-CC and ZZ-NC are enough similar; however, the use of ammonia carbonate rather than sodium bicarbonate seems to confer a higher development of surface area (*SA*, 305 *vs.* 288 m^2/g) and higher porosity (*PV*, 0.281 *vs.* 0.270 cm^3/g). Moreover, the micropore volume of the samples appears quite similar (V_{micro}, 0.111–0.113 cm^3/g), without any significant decrease upon precipitation of the methanol catalyst precursors on H-ZSM5 (V_{micro}, 0.115 cm^3/g), indicating that the microporous structure of the zeolite remains substantially unchanged.

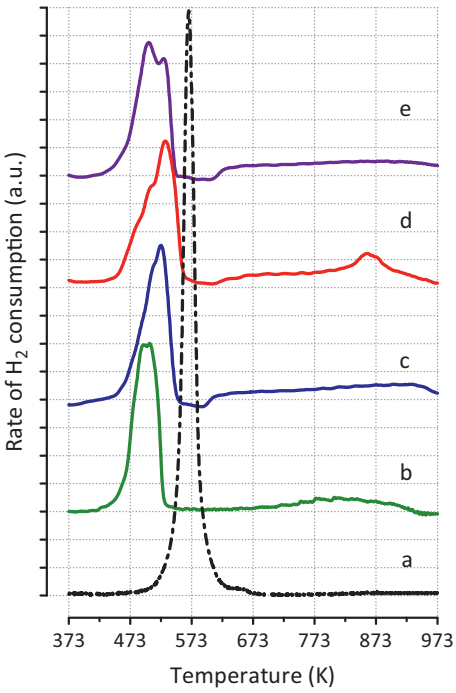

Fig. 1. H_2-TPR profiles of the investigated catalysts: (a) CuO; (b) ZZ-CC; (c) ZZ-NC; (d) ZZ-OC; (e) ZZ-UH.

3.2. Structural and morphological properties

The reducibility of the samples was studied by H_2-TPR measurements. The corresponding reduction profiles of all prepared systems are shown in Fig. 1, while the quantitative data, in terms of onset reduction temperature ($T_{o,red}$), temperature of peak maxima (T_{Mi}) and extent of hydrogen consumption are reported in Table 2.

Compared to pure CuO, which exhibits a sharp reduction peak at a temperature of 573 K, the reduction behavior of the prepared catalysts differs both in terms of shape and reduction temperature of peaks. All the systems display a main peak centered between 490 and 526 K, that results more or less asymmetric or split in two peaks for some sample. In fact, the ZZ-CC catalyst displays a symmetric peak, but with two reduction maxima clearly visible (T_{M1}, 490 K and T_{M2}, 498 K). The other samples exhibit a pattern characterized by one reduction maximum shouldered either at lower temperature, like ZZ-NC (T_{M1}, 510 K) and ZZ-OC (T_{M1}, 502 K), or at higher temperature, like ZZ-UH (T_{M2}, 526 K).

For all the catalyst samples, within the temperature range 373–623 K, H_2/Cu ratios higher than 1 (H_2/Cu, 1.03–1.24) should be diagnostic of a full reduction of CuO to Cu^0, associated with an incipient reduction of ZnO and/or ZrO_2 in interaction with copper crystallites [15]. The presence of shoulders should also indicate

Table 1
Chemical composition and textural properties of the catalytic systems.

Sample	CuO (wt.%)	ZnO	ZrO_2	SiO_2	Al_2O_3	SA[a] (m^2/g)	PV (cm^3/g)	V_{micro} (cm^3/g)
H-ZSM5	–	–	–	94.6	5.4	317 ± 6	0.315	0.115
ZZ-CC[b]	21.0	7.5	21.8	45.4	2.6	288 ± 3	0.270	0.111
ZZ-NC	20.9	7.6	22.0	46.9	2.7	305 ± 6	0.281	0.111
ZZ-OC	21.2	7.7	21.9	46.6	2.6	248 ± 3	0.261	0.113
ZZ-UH	21.0	7.6	22.0	46.8	2.6	372 ± 9	0.286	0.112

[a] Langmuir model, considering monolayer gas adsorption.
[b] Na content, 1.6 wt.%.

different Cu species and therefore inhomogeneous distribution of CuO.

Basically, the shoulders at lower temperatures can be ascribed to the reduction of well-dispersed CuO, while the main peak is attributed to the reduction of bulk CuO [26,27]. Instead, in the cases of shoulders at higher temperature, there might be a consecutive reduction of Cu^{2+} to $Cu^{\delta+}$ and finally to Cu^0 [27].

It is relevant that a hard reduction of CuO occurs for the ZZ-OC sample (d), having a higher $T_{o,red}$ of 428 K, likely due to the preparation procedure of such a system that could hinders the reactivity of the surface Cu^{2+} species [15]. Furthermore, a baseline drift at $T > 623$ K, with a poorly pronounced maximum at 845–923 K, monitors the reduction of ZnO and/or decomposition of residual species coming from precursors [19] in a more or less strong extent of interaction with the acidic functions of the zeolite in the hybrid systems [28–30].

The diffraction patterns of the reduced catalysts are shown in Fig. 2.

In all the samples, the intensities of diffraction peaks ascribed to H-ZSM5 between 5° and 10° (JCPDS 44-0003) appear similar, which indicates that the structure of zeolite was well-preserved after chemical interaction with Cu, Zn and Zr precursors.

The presence of ZrO_2 in the precursors is manifested by a peak at $2\theta \approx 30°$ (JCPDS 24-1164), whereas the peaks assigned to ZnO can be seen at 36° and 47° (JCPDS 36-1451). The peak located at about 43° is diagnostic of the presence of metallic copper (JCPDS 01-089-2838), although on ZZ-NC and ZZ-UH this peak appears narrower than on ZZ-CC and ZZ-UH.

These differences might be related not only to the preparation method, but also to the extent of reduction, that, for example, in the case of the gel-oxalate coprecipitated sample, results to be lower than the other catalysts (see Table 2). In fact, differently from the other samples, in the ZZ-OC catalyst two diffraction peaks, corresponding to planes (−1 1 1) and (1 1 1) of CuO crystallized in

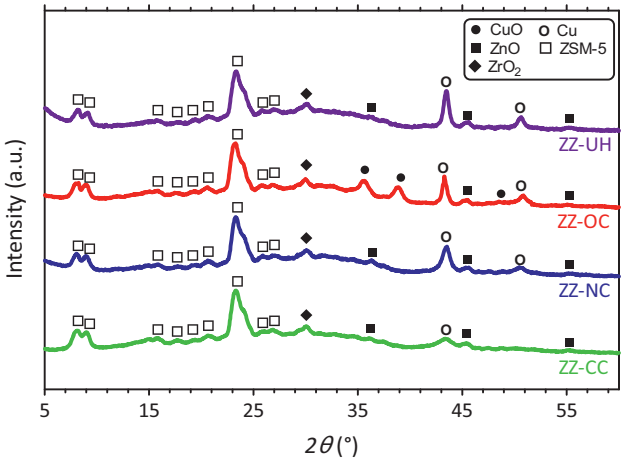

Fig. 2. XRD patterns of the reduced catalysts.

Table 2
Quantitative data of H_2-TPR.

Sample	$T_{o,red}$ (K)	T_{M1} (K)	T_{M2} (K)	H_2 consumption[a] ($mmol/g_{cat}$)	H_2/Cu[a]
ZZ-CC	416	490	498	3.27	1.24
ZZ-NC	391	510	519	3.17	1.20
ZZ-OC	428	502	526	2.72	1.03
ZZ-UH	403	498	520	3.06	1.16

[a] In the T range, 273–623 K.

monoclinic structure (JCPDS 05-0661) appear also visible at 35.5° and 39°, respectively. Based on the XRD results, it seems to understand that, depending on different preparation method, a different degree of aggregation or growth of Cu crystallite is obtainable.

In order to study the influence of preparation method along with the distribution of copper, zinc and zirconium on H-ZSM5, SEM-EDAX analysis has been carried out. The results obtained are shown in Fig. 3.

From images, it is possible to observe that ZZ-CC and ZZ-NC samples present a similar morphology, characterized by spherical particles of ca. 30–40 nm. Such a morphological homogeneity, in terms of uniform distribution of elements per unit of surface, should be the result of the coprecipitation performed under ultrasound irradiation that, as shown from the results of the elemental chemical mapping, favors a better mixing among the precursors, also enhancing their distribution onto the zeolite framework. In particular, when ammonia carbonate is used instead of sodium bicarbonate as the precipitating agent, a higher extent of homogenization among the elements seems to be evident (see Fig. 3B), likely induced by the evolution of ammonia and CO_2 during calcination, that also confers a higher porosity (see Table 1). The SEM images of the ZZ-OC sample show the formation of large clusters together with compact particles, while on the ZZ-UH catalyst a sponge-like morphology is observable, with particles larger than those of the other samples and rhomboidal in shape, so accounting for a higher development of surface area ($372\ m^2/g$) and porosity ($0.186\ cm^3/g$), as reported in Table 2. However, the elemental mapping performed on these two systems reveals a poor homogenization of precursors, so denoting the lack of an uniform long-range distribution on the zeolite.

The results of pulse chemisorption with N_2O, in terms of Cu surface area (S_{Cu}), metal dispersion (D_{Cu}) and crystallite size (d_{Cu}), are summarized in Table 3. The Table also reports the copper crystallite sizes as calculated by Scherrer equation using the XRD peak at $2\theta \approx 43°$.

The ZZ-OC sample presents the lowest values of Cu surface area ($6.7\ m^2/g$) and metal dispersion (5.4%), while the other systems exhibit similar values, with specific Cu surface area comprised between 8.7 and $10.2\ m^2/g$, dispersion of about 7–8% and crystallite sizes of 13–15 nm. The ZZ-CC and ZZ-NC systems exhibit smaller Cu particles, whereas ZZ-OC and ZZ-UH samples are characterized by larger particle size, according to the following order:

ZZ-CC < ZZ-NC < ZZ-UH < ZZ-OC

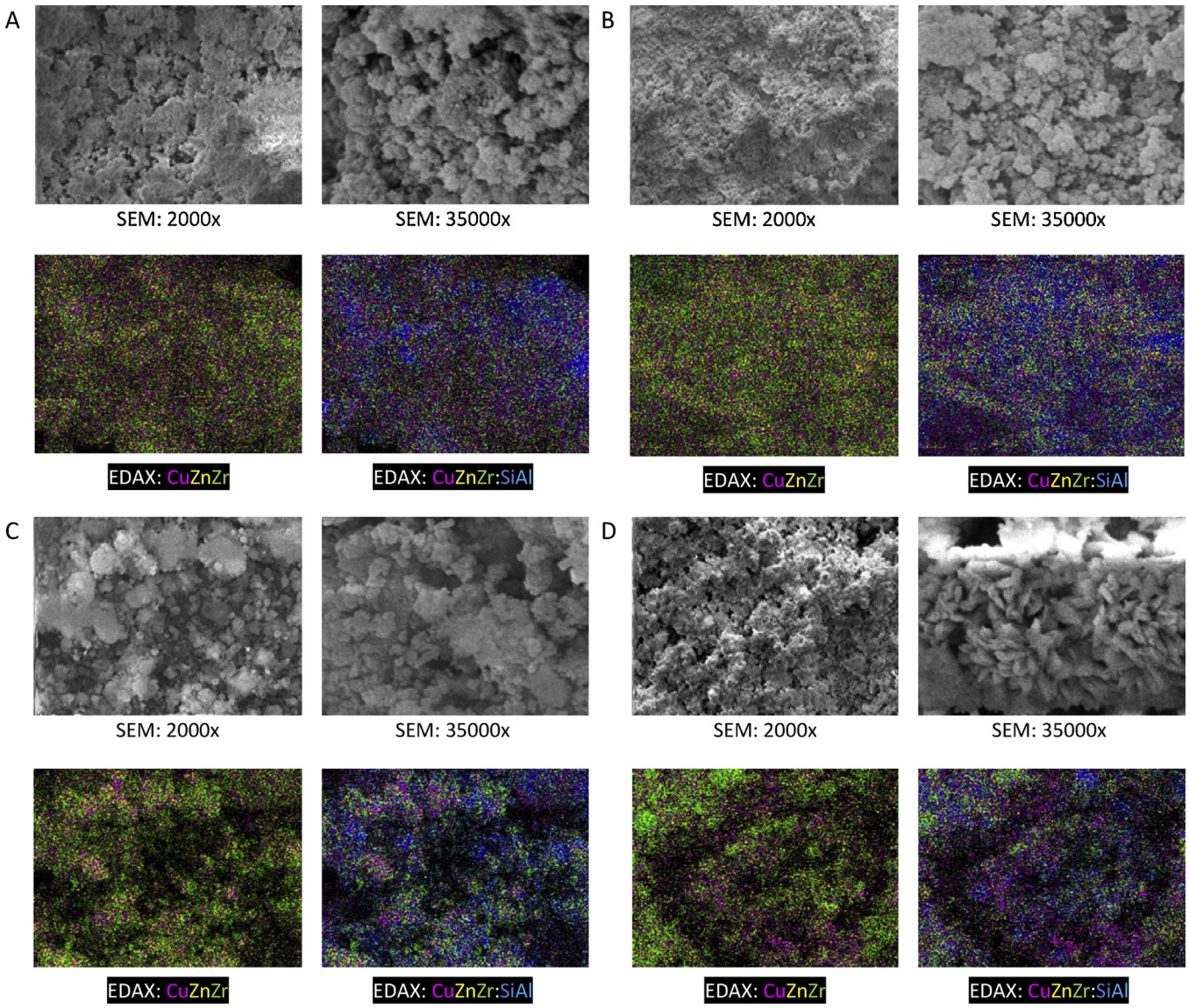

Fig. 3. SEM images at different magnification and EDAX mapping on the studied systems: (A) ZZ-CC; (B) ZZ-NC; (C) ZZ-OC; (D) ZZ-UH.

The crystallites size calculated by Scherrer equation (see Table 3) increases in the same order and, in absolute terms, only a slight difference with the values determined from N_2O-pulse chemisorption can be observed.

Therefore, the data reported should be considered reliable enough, since a general trend becomes visible. Still, the lowest metal surface area of gel-oxalate coprecipitated catalyst (ZZ-OC) could be the result of an incomplete reduction of CuO species, so also accounting for a lower copper dispersion. These findings are well explained by the relationships between H_2 consumption and Cu surface area shown in Fig. 4: the development of metal surface area (and also, the dispersion) are a direct function of the reducibility of the sample.

In order to shed lights on the role of both basic and acidic sites involved in DME synthesis reaction, also determining the

Table 3
Metal properties of the samples as determined by different characterization techniques.

Sample	N_2O chemisorption			XRD measurements	
	S_{Cu} (m^2/g)	D_{Cu} (%)	d_{Cu} (nm)	2θ (°)	d_{Cu} (nm)
ZZ-CC	10.2	8.1	13	43.32	7
ZZ-NC	9.3	7.6	14	43.42	12
ZZ-OC	6.7	5.4	19	43.20	20
ZZ-UH	8.7	7.1	15	43.43	19

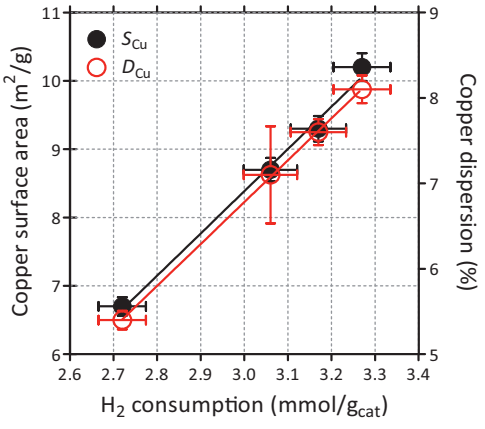

Fig. 4. Copper surface area and dispersion as a function of reducibility.

Table 4
Quantitative data of NH_3 and CO_2 chemisorption measurements.

Sample	NH_3-uptake ($\mu mol/g_{cat}$)	T_{d1,NH_3} [a] (K)	T_{d2,NH_3} [b] (K)	T_{d3,NH_3} [c] (K)	CO_2-uptake ($\mu mol/g_{cat}$)	T_{d1,CO_2} [d] (K)	T_{d2,CO_2} [e] (K)
ZZ-CC	67.0	470	587	–	40.0	–	466
ZZ-NC	379.0	500	613	813	28.8	372	488
ZZ-OC	404.2	510	676	808	17.3	361	448
ZZ-UH	300.0	484	665	782	24.7	–	475
H-ZSM5	880.0	493	690	–	1.6	–	522

[a] T_{d1,NH_3}, temperature of maximum desorption of NH_3 between 373 and 573 K.
[b] T_{d2,NH_3}, temperature of maximum desorption of NH_3 between 573 and 773 K.
[c] T_{d3,NH_3}, temperature of maximum desorption of NH_3 between 773 and 973 K.
[d] T_{d1,CO_2}, temperature of maximum desorption of CO_2 between 273 and 413 K.
[e] T_{d2,CO_2}, temperature of maximum desorption of CO_2 between 413 and 623 K.

abundance of the surface adsorption sites on the various investigated catalysts, a TPD study of NH_3 and CO_2 was carried out. The desorption profiles are shown in Fig. 5 and quantitative data reported in Table 4.

The H-ZSM5 zeolite, used as the methanol dehydration component in the prepared catalysts, exhibited a total NH_3-uptake of 880 μmol/g. As it is possible to observe, the zeolite (a) shows two desorption peaks, indicating the existence of at least two types of acid sites: the first one (between 373 and 573 K) is normally attributed to the desorption of weakly bound ammonia. The second peak, in the temperature region between 573 and 873 K, is usually attributed to the ammonia desorbed from the Brønsted acid sites [31–33]. The profiles of catalysts are also characterized by a main low temperature peak, associated to ammonia desorbed from weak acidic sites, with a minor contribution of stronger acid sites, belonging either to the zeolite framework ($T_{d,NH3}$, 693 K) or to extra-framework Brønsted acid sites ($T_{d,NH3}$ > 773 K). With an uptake of 404 μmol/g (see Table 4), ZZ-OC presents the highest number of acidic sites. Since more than 60% of NH_3 desorption takes place at temperatures below 623 K (profile *d*), most of them can be considered as weak sites, although in this sample a discrete amount (ca. 35%) of acid sites of moderate strength is also present.

On the contrary, ZZ-CC is characterized by a low acidity, mainly assignable to the presence of weak acid sites. With similar desorption patterns, the NH_3 uptakes of ZZ-NC and ZZ-UH samples result to be 379 and 300 μmol/g, respectively. On the whole, the differences in the total acidity of all the samples could be explained considering that, like for similar metal–oxide/zeolite catalysts [34,35], CuO, ZnO and ZrO_2 might migrate onto the zeolite leading to a blockage of acid sites. On this account, García-Trenco et al. [34] also used EPR-experiments to show that Cu^{2+} can migrate to the zeolite, exchanging with zeolite protons, so leading to a decrease in Brønsted-acidity.

As regards the basic properties, due to the variables adopted during preparation, the CO_2-TPD profiles (see Fig. 5B) disclose a different concentration of surface basic sites on the various samples. In fact, although recent density functional theory calculations pointed out a highly positive binding energy that leads to very unstable chemisorption of CO_2 on Cu [36], it is known that not only zirconia possesses surface Lewis basic sites able to adsorb CO_2, but also ZnO should contribute to enhance the affinity of the systems to CO_2 absorption [37–39]. So, despite an irrelevant CO_2 uptake on the pure zeolite (1.6 $\mu mol/g_{cat}$), the CO_2-TPD patterns of the ZZ-NC and ZZ-UH systems (Fig. 5B) show fundamentally a desorption profile with a main maximum between 460 and 480 K, similar in qualitative (Fig. 5A, patterns *c*–*e*) and quantitative terms (28.8 and 24.7 $\mu mol/g_{cat}$, respectively). Indeed, the ZZ-OC catalyst exhibits a minor CO_2 uptake (17.3 $\mu mol/g_{cat}$) with the maximum

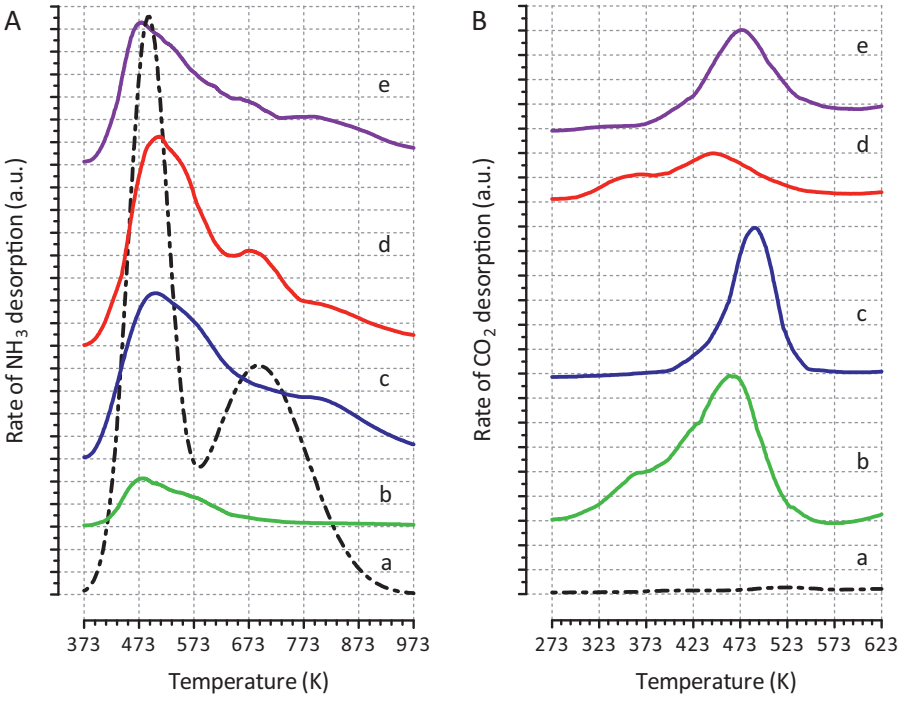

Fig. 5. NH_3-TPD (A) and CO_2-TPD (B) profiles of the various pre-reduced catalysts: (a) H-ZSM5; (b) ZZ-CC; (c) ZZ-NC; (d) ZZ-OC; (e) ZZ-UH.

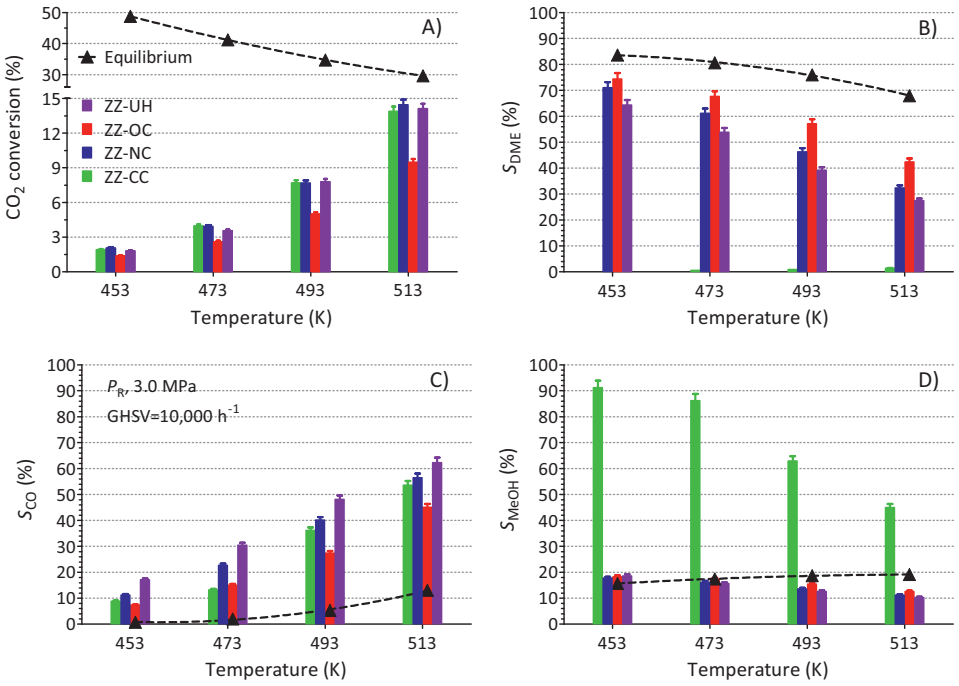

Fig. 6. Conversion of CO_2 (A) and selectivity to DME (B), CO (C) and MeOH (D) in the CO_2 hydrogenation reaction (H_2/CO_2, 3 mol/mol).

shifted at lower temperature, whereas the highest coverage of CO_2 (40.0 μmol/g_{cat}) is recorded on the ZZ-CC sample, where the large population of basic sites centered at around 466 K can be associated with the coprecipitation procedure by sodium bicarbonate that, although the accurate washing step, finally contains residual Na (see Table 1), so likely conferring a more basic character.

Usually, the weak basic sites may be ascribed to the linear adsorption of CO_2 while the strong basic sites may result from the bridge adsorption of CO_2 [40]. Moreover, mainly for ZZ-CC and ZZ-OC, the maximum temperature results to be tailed on the low temperature side, exhibiting a broad and poorly resolved component with maximum at ca. 360 K, monitoring mostly the surface basic sites of the zirconia carrier [37–39,41–44].

3.3. Catalytic results

The CO_2 hydrogenation activity data, at reaction temperature ranging from 473 to 513 K, pressure 3.0 MPa and space velocity of 10,000 h^{-1}, are shown in Fig. 6, in terms of CO_2 conversion (A) and selectivity to DME (B), CO (C) and MeOH (D).

Irrespective of the preparation method, it is possible to observe that all the systems work under a prevailing kinetic regime, with CO_2 conversion values always lower than that expected from thermodynamic equilibrium data, at any reaction temperature.

All systems show no significant difference in terms of CO_2 conversion at low temperatures (453–473 K), whereas at higher temperature the minor activity of the ZZ-OC sample in respect of the other systems appears to be evident. In fact, at 513 K the gel-oxalate ZZ-OC coprecipitated catalyst reaches a maximum value of CO_2 conversion of 9.5%, which is about 40% lower than that obtained with other catalysts. However, a much more significant difference in catalytic behavior can be deduced by comparing the results in terms of selectivity. In fact, ZZ-CC, for example, exhibits a near-zero DME selectivity at any temperature, while CO progressively increases with temperature (from 9 to 54%) in correspondence of the decreasing of methanol selectivity from 91 to 45% in all the temperature range investigated. This behavior, can be explained considering the lowest acidity of such sample (67 μmol NH_3/g, see Table 4).

Regarding the other systems, methanol formation approaches the equilibrium level at any reaction temperature, while the DME selectivity decreases with temperature in correspondence of a progressive increasing of CO formation. Specifically, the DME selectivity of ZZ-NC is offset by CO selectivity values increasing from 11 to 56%, while at a lower DME formation of ZZ-UH (64 → 27%) corresponds a higher CO formation at any reaction temperature (17 → 62%). The minor DME selectivity of ZZ-UH compared to

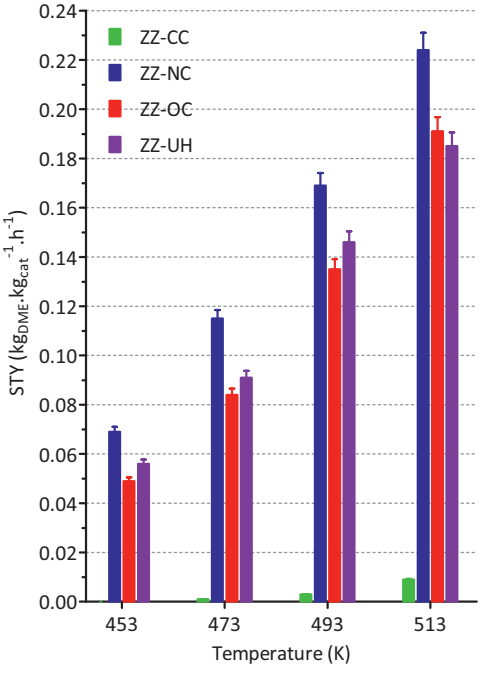

Fig. 7. DME productivity in the T_R range 453–513 K (P_R, 3.0 MPa; GHSV, 10,000 h^{-1}; H_2/CO_2, 3 mol/mol).

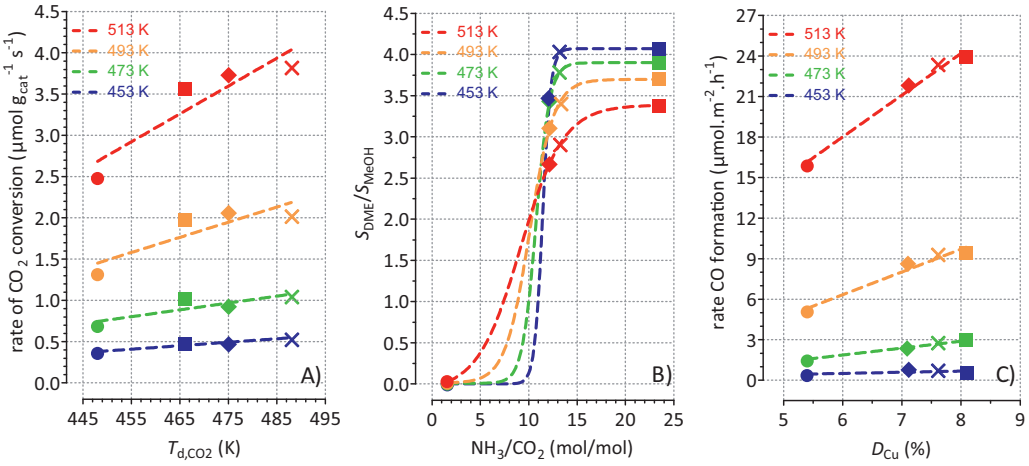

Fig. 8. (A) Influence of temperature of CO_2 desorption (T_{d,CO_2}) on the rate of CO_2 conversion; (B) fitting of DME-to-MeOH selectivity ratio (S_{DME}/S_{MeOH}) as a function of NH_3-to-CO_2 chemisorption ratio; (C) influence of copper dispersion (D_{Cu}) on the specific rate of CO formation. Catalysts: ■ ZZ-CC; × ZZ-NC; ● ZZ-OC; ♦ZZ-UH.

ZZ-NC could be justified considering that the catalyst prepared by urea hydrolysis, not only has fewer acid sites, but the highest surface area of such system could facilitate the occurrence of side reactions (*e.g.*, RWGS, DME/CH_3OH decomposition, etc. . .), since a higher probability of adsorption phenomena on the catalyst surface reflects possible changes in selectivity due to parallel as well as consecutive reaction paths.

Despite a minor CO_2 conversion, at any reaction temperature, the ZZ-OC sample exhibits the highest values of DME selectivity (74 → 42%) and the lowest values of CO (7 → 45%). In any case, the CO selectivity values higher than the equilibrium ones confirm that, under the reaction conditions, the hydrogenation of CO_2 runs in a predominantly kinetic regime.

On the whole, if a lesser reducibility (see Table 2) or lower metal dispersion (Table 3) of catalyst accounts for a minor activity toward the CO_2 conversion, however, the achievement of high DME selectivity depends both on catalyst acidity, which promote the methanol dehydration reaction, and on a low concentration of metallic sites, which could be responsible for DME/MeOH decomposition.

By rationalizing the results in terms of DME productivity, the catalytic pattern of the studied systems depicts a straight increase in DME productivity (*STY*) with temperature, as shown in Fig. 7. With the exception of the ZZ-CC sample that exhibits good activity in CO_2 conversion but poor selectivity to DME (low acidity, see Table 4), the best performance at any temperature is shown by ZZ-NC sample reaching a maximum value of 0.225 $kg_{DME}/kg_{cat}/h^{-1}$ at 513 K.

3.4. Structure–reactivity relationships

From a preliminary evaluation of data, the reactivity scale of the investigated systems seems to be directly related neither to total surface area or metal Cu exposure or surface basicity or surface acidity. In fact, no direct relationships between STY_{DME} of the catalysts with one of these properties can be found. This should indicate that the CO_2-to-DME functionality is not governed by a single parameter, rather a concurrence of textural, structural or surface factors must be taken into account. So, in the attempt to rationalize the catalytic behavior, some correlations that could describe the key factors governing CO_2 activation and DME/CO formation were considered (see Fig. 8).

From Fig. 8A it emerges that, at any investigated temperature, the rate of CO_2 conversion almost linearly increases with the temperature of CO_2 desorption, so that in the presence of strong basic sites the CO_2 activation should be favoured.

Moreover, from Fig. 8B it is observable that in presence of a limited number of acid sites (low NH_3/CO_2 ratio), there is no formation of DME since the dehydration reaction of MeOH to DME is not favoured.

Increasing the concentration of the acid sites, a gradual increasing in the S_{DME}/S_{MeOH} ratio is observed, until the DME/MeOH ratio no longer changes as the NH_3/CO_2 ratio increases. It seems to observe the evolution of an acid–base titration in which, over the equivalence point (in this case a concentration of acid sites about 10 times higher than the basic sites), methanol is continuously dehydrated to DME. However, the temperature plays a negative role on this selectivity trend considering that DME formation is an exothermic reaction [14].

Finally, in Fig. 8C the CO formation rate results a linear function of the Cu dispersion. Indeed, as the reaction proceeds, owing to the formation of oxygen-containing products (such as C—O, H—O, C—O—H, . . ., species), the copper particles of smaller size are more ready toward the re-oxidation, likely forming $Cu^{\delta+}$ species, considered more active in CO formation [37,45]. Really, this insight appears to be more evident at high temperature (>473 K), when the secondary reactions, either the methanol-to-CO decomposition or RWGS are more favoured than the CO_2 hydrogenation reaction.

Therefore, these findings further confirm that the direct CO_2-to-DME hydrogenation on Cu–ZnO–ZrO_2/H-ZSM5 systems is to be considered a multi-site reaction, taking place with the primary formation of methanol, while DME is consecutively formed on the acid sites of the zeolite framework from methanol dehydration. Indeed, H_2 is initially adsorbed and activated (H_2^*) on the Cu^0 sites resulting from the reduction of copper species, whereas CO_2 is bridged-adsorbed [17,40] on basic sites (ZnO and ZrO_2 surface sites) to form activated CO_2 (CO_2^*). By spillover, H_2^* reaches CO_2^* giving rise to the formation of intermediate species (*i.e.*, formate/dioxomethylene/methoxy) [15,37,45], that are stabilized in proximity of the metal–oxide interface [15,19,45] prior to further evolve to methanol by hydrogenation. As a consequence, also the role of $Cu^{\delta+}$ sites, located at the interface between Cu^0 and basic sites (ZnO and/or ZrO_2), must be considered.

Summarizing, to design an efficient catalyst for the production of DME in a single-step from CO_2-H_2 mixtures, a balanced distribution of different sites on catalyst surface becomes determinant. This concept allows to justify why, among the different catalysts prepared, ZZ-NC is the most active and selective system. In fact, as also demonstrated by SEM-EDAX analysis (see Fig. 3), this catalyst, due

to sono-chemical irradiation during preparation, presents a long-range "homogeneity", both in terms of morphology and sites distribution, with a proper balance between metallic and acid–base sites.

4. Conclusions

In this work the nature of surface adsorption sites and reactivity pattern of multifunctional Cu–ZnO–ZrO_2/H-ZSM5 catalysts for the "one-step" CO_2-to-DME hydrogenation reaction was investigated. In such systems, an integrated generation of active sites was realized in a slurry medium, so that the source of the catalytic functionality, usually attributed to two parent catalysts (*i.e.*, methanol catalyst and zeolite), cannot be distinguishable. The use of different precipitating agents significantly affects the physico-chemical properties of the multi-functional systems as well as the catalytic performance in the CO_2-to-DME hydrogenation reaction. The coprecipitation of the methanol synthesis catalyst on the zeolite particles under ultrasound irradiation favours a better mixing among the precursors, also enhancing their distribution into the zeolite framework. The decrease in acidity after coprecipitation–deposition was explained considering that metal ions might migrate onto the zeolite leading to an exchange with zeolite protons.

The CO_2-to-DME hydrogenation functionality was related to a "multisite" reaction path, involving a mix of surface sites necessary for the primary formation of methanol, upon adsorption/activation of H_2 (on metal Cu sites) and CO_2 (on strong basic sites), followed by its dehydration to DME on acid sites of the zeolite. The copper particle size was found to be crucial in order to prevent the occurrence of side reactions. Overall, to design an efficient multi-functional system for the production of DME from CO_2, the concurrence of textural, structural and surface factors must be adequately balanced.

Acknowledgements

This work was financially supported by the Italian Research Fund (PON R&C 2007-2013, DD 713/Ric. 29.10.2010, PON02_00451_3362376) through the "BIO4BIO" project, Biomolecular and Energy valorization of residual biomass from Agroindustry and Fishing Industry.

References

[1] G. Centi, S. Perathoner, Catal. Today 148 (2009) 191–205.
[2] K.M. Yu, I. Curcic, J. Gabriel, S.C. Tsang, ChemSusChem 1 (2008) 893–899.
[3] B. Li, Y. Duan, D. Luebke, B. Morreale, Appl. Energy 102 (2013) 1439–1447.
[4] R. Steeneveldt, B. Berger, T.A. Torp, Chem. Eng. Res. Des. 84 (2006) 739–763.
[5] T. Semelsberger, R. Borup, H. Greene, J. Power Sources 156 (2006) 497–511.
[6] G. Olah, A. Goeppert, G.K. Surya Prakash, J. Org. Chem. 74 (2009) 487–498.
[7] F. Frusteri, L. Spadaro, O. Di Blasi, G. Bonura, F. Arena, European Automobile Engineers Cooperation—10th EAEC European Automotive Congress 2 (2005) 588–599.
[8] Y. Zhu, S. Wang, X. Ge, Q. Liu, Z. Luo, K. Cen, Fuel Process. Technol. 91 (2010) 424–429.
[9] J.W. Bae, S.H. Kang, Y.J. Lee, K.W. Jun, J. Ind. Eng. Chem. 15 (2009) 566–572.
[10] L.A. Pellegrini, G. Soave, S. Gamba, S. Lange, Appl. Energy 88 (2011) 4891–4897.
[11] G. Jia, Y. Tan, Y. Han, Ind. Eng. Chem. Res. 45 (2006) 1152–1159.
[12] S.P. Naik, H. Du, H. Wan, V. Bui, J.D. Miller, W.W. Zmierczak, Ind. Eng. Chem. Res. 47 (2008) 9791–9794.
[13] F. Arena, L. Spadaro, O. Di Blasi, G. Bonura, F. Frusteri, Stud. Surf. Sci. Catal. 147 (2004) 385–390.
[14] G. Bonura, M. Cordaro, L. Spadaro, C. Cannilla, F. Arena, F. Frusteri, Appl. Catal., B: Environ. 140–141 (2013) 16–24.
[15] G. Bonura, M. Cordaro, C. Cannilla, F. Arena, F. Frusteri, Appl. Catal., B: Environ. 152–153 (2014) 152–161.
[16] G. Bonura, F. Arena, G. Mezzatesta, C. Cannilla, L. Spadaro, F. Frusteri, Catal. Today 171 (2011) 251–256.
[17] F. Arena, G. Italiano, K. Barbera, G. Bonura, L. Spadaro, F. Frusteri, Catal. Today 143 (2009) 80–85.
[18] F. Arena, G. Italiano, K. Barbera, S. Bordiga, G. Bonura, L. Spadaro, F. Frusteri, Appl. Catal., A: Gen. 350 (2008) 16–23.
[19] F. Arena, K. Barbera, G. Italiano, G. Bonura, L. Spadaro, F. Frusteri, J. Catal. 249 (2007) 185–194.
[20] R. Ahmad, D. Schrempp, S. Behrens, J. Sauer, M. Döring, U. Arnold, Fuel Process. Technol. 121 (2014) 38–46.
[21] R. Khoshbin, M. Haghighi, Chem. Eng. Res. Des. 91 (2013) 1111–1122.
[22] A. García-Trenco, S. Valencia, A. Martínez, Appl. Catal., A: Gen. 468 (2013) 102–111.
[23] S. Allahyari, M. Haghighi, A. Ebadi, S. Hosseinzadeh, Energy Convers. Manage. 83 (2014) 212–222.
[24] Q. Sun, Y.L. Zhang, H.Y. Chen, J.F. Deng, D. Wu, S.Y. Chen, J. Catal. 167 (1997) 92–105.
[25] J.W. Evans, M.S. Wainwright, A.J. Bridgewater, D.J. Young, Appl. Catal. 7 (1983) 75–83.
[26] M. Shimokawabe, H. Asakawa, N. Takezawa, Appl. Catal. 59 (1990) 45–58.
[27] X.J. Tang, J.H. Fei, Z.Y. Hou, X.M. Zheng, H. Lou, Energy Fuels 22 (2008) 2877–2884.
[28] T. Tagawa, M. Ito, S. Goto, Appl. Organomet. Chem. 15 (2001) 127–134.
[29] G.R. Moradi, M. Nazari, F. Yaripour, Fuel Process. Technol. 89 (2008) 1287–1296.
[30] B.O. Hincapie, L.J. Garces, S. Gomez, R. Ghosh, S.L. Suib, Catal. Today 110 (2005) 323–329.
[31] M. Niwa, N. Katada, Catal. Surv. Jpn. 1 (1997) 215–226.
[32] L. Rodríguez-González, F. Hermes, M. Bertmer, E. Rodríguez-Castellón, A. Jiménez-López, U. Simon, Appl. Catal., A: Gen. 328 (2007) 174–182.
[33] N. Katada, H. Igi, J. Kim, M. Niwa, J. Phys. Chem. B 110 (1997) 5969–5977.
[34] A. García-Trenco, A. Vidal-Moya, A. Martínez, Catal. Today 179 (2012) 43–51.
[35] J.H. Flores, M.I. Pais da Silva, Colloids Surf., A: Physicochem. Eng. Aspects 322 (2008) 113–123.
[36] S.G. Wang, X.Y. Liao, D.B. Cao, C.F. Huo, Y.W. Li, J. Wang, H. Jiao, J. Phys. Chem. C 111 (2007) 16934–16940.
[37] I.A. Fisher, A.T. Bell, J. Catal. 178 (1998) 153–173.
[38] J. Wambach, A. Baiker, A. Wokaun, Phys. Chem. Chem. Phys. 1 (1999) 5071–5080.
[39] K. Pokrovski, K.T. Jung, A.T. Bell, Langmuir 17 (2001) 4297–4303.
[40] L. Zhang, Y. Zhang, S. Chen, Appl. Catal., A: Gen. 415–416 (2012) 118–123.
[41] J. Słoczyński, R. Grabowski, P. Olszewski, A. Kozłowska, J. Stoch, M. Lachowska, J. Skrzypek, Appl. Catal., A: Gen. 310 (2006) 127–137.
[42] C. Schild, A. Wokaun, A. Baiker, J. Mol. Catal. 63 (1990) 223–242.
[43] X.M. Liu, G.Q. Lu, Z.-F. Yan, Appl. Catal., A: Gen. 279 (2005) 241–245.
[44] Z.-Y. Ma, C. Yang, W. Wei, W.-H. Li, Y.-H. Sun, J. Mol. Catal. A: Chem. 227 (2005) 119–124.
[45] F. Arena, G. Mezzatesta, G. Zafarana, G. Trunfio, F. Frusteri, L. Spadaro, J. Catal. 300 (2013) 141–151.